Talanta 134 (2015) 317–324

Contents lists available at ScienceDirect

Talanta

journal homepage: www.elsevier.com/locate/talanta

ZnS:Mn nanoparticles functionalized by PAMAM-OH dendrimer based fluorescence ratiometric probe for cadmium

Bruno B. Campos [a], Manuel Algarra [b,*], Ksenija Radotić [c], Dragosav Mutavdžić [c], Enrique Rodríguez-Castellón [b], José Jiménez-Jiménez [b], Beatriz Alonso [d], Carmen M. Casado [d], Joaquim C.G. Esteves da Silva [a]

[a] Centro de Investigação em Química, Departamento de Química e Bioquímica, Faculdade de Ciências da Universidade do Porto, Porto, Portugal
[b] Departamento de Química Inorgánica, Facultad de Ciencias, Universidad de Málaga, Campus de Teatinos s/n, 29071 Málaga, Spain
[c] Institute for Multidisciplinary Research, University of Belgrade, KnezaViševeslava 1, 11000 Beograd, Serbia
[d] Departamento de Química Inorgánica, Universidad Autónoma de Madrid, Cantoblanco, 28049 Madrid, Spain

ARTICLE INFO

Article history:
Received 8 July 2014
Received in revised form
3 October 2014
Accepted 8 October 2014
Available online 24 November 2014

Keywords:
Dendrimer
Quantum dots
ZnS:Mn^{2+}
Ratiometric sensor
Cadmium

ABSTRACT

We report a nanocomposite of ZnS:Mn quantum dots and a third generation PAMAM-OH dendrimer (ZnS:Mn@PAMAM-$OH_{G=3}$) which was rationalized to be used as ratiometric nanosensor for Cd^{2+} in aqueous solution. The nanoparticles exhibited a bright yellow-orange emission with peaks at 448 and 595 nm. The structure of ZnS:Mn was not changed after coupling with PAMAM-OH, which was evidenced by the analysis of the emission spectra of the compounds. The results confirm that the prepared fluorescence nanoparticles could selectively detect Cd^{2+} in aqueous solution with a limit of detection of 24.34 μM and RSD 4.07%, obtained by using the ratio I_{448}/I_{595}. The method was applied to different water samples.

1. Introduction

The synthesis of doped quantum dots (QDs) allows the development of nanomaterials with different and improved properties, when compared with the raw QDs, and is receiving much attention [1–6]. A favorable system to be doped is zinc sulfide fluorescent nanoparticles (ZnS QDs) by Mn^{2+} ions, which confers characteristic emission independent of the size of the nanoparticle, due to the lower lying states of Mn^{2+} ions ($^4T_1 \rightarrow {}^6A_1$) [7], permitting larger Stokes shift to avoid self-absorption, longer excited state lifetime, enhanced thermal and chemical stabilities, and minimized toxicity [8–15].

ZnS nanocrystals doped with manganese ions (ZnS:Mn) have attracted great interest on account of their high quantum efficiency and thermal stability, essential properties for chemical applications such as chemical and biosensor, molecular imaging, monitoring drug delivery, etc. [16–20].These properties can be improved substantially by modifying their surfaces with increasing quantum efficiency and stability; therefore ZnS:Mn has been conjugated with different ligand exchange coating agents such as glucose oxidase, for glucose biosensor in biological fluids [21], polyethyleneimine, for heparin assay [22], thioglycerol, for bioimaging [23], chitosan and PEG, for bio-labelling [24,25].

Besides all these nanocomposites materials, dendrimer derivates have been recently exploited for coatings of nanoparticles surfaces which can alter the charge, functionality and reactivity. Simultaneously, the coupling of QDs with dendrimers enhances the stability and dispersion of the nanoparticles as demonstrated by previous results showing that, the dendrimers functionalized CdSe and ZnSe QDs, enhanced their behavior in aqueous solution for quantification of heavy metals and C-Reactive Protein, respectively by means the quenching effect caused to the emission of QDs [26,27]. In the literature, just a few works are found involving fluorescent semiconductors and the terminated OH-poly(amidoamine) dendrimer (PAMAM-OH). As example, CdS QDs were synthesized by using hydroxyl-terminated PAMAM dendrimers as templates and investigated the effects of Cd^{2+} ion/dendrimer ratio, dendrimer generations, and temperatures on the resultant CdS QDs [28]. Due to the harmful cumulative effect of cadmium-containing QDs in the human body [29], arouse a major interest in less toxic fluorescent nanoparticles.

In this work a novel ratiometric chemical nanosensor for Cd^{2+} ions based on terminated OH-poly(amidoamine) dendrimer (PAMAM-OH) of third generation was developed. This nanosensor

* Corresponding author. Tel.: +34 952 131873; fax: +34 952 132000.
E-mail address: malgarra67@gmail.com (M. Algarra).

http://dx.doi.org/10.1016/j.talanta.2014.10.010
0039-9140/

resulted from the research of two different families of dendrimers, functionalized ZnS:Mn QDs, (ZnS:Mn@PAMAM-$OH_{G=3}$). The presence of this ion in the environment raises human health concerns. This Cd^{2+} nanosensor shows minimal interference of environmental conditions when competing with other species, and in the presence of Cd^{2+} an enhancement of the fluorescent intensity is observed. This ratiometric nanosensor, based on QDs functionalized dendrimer, is the first attempt with this of nanomaterial [30,31].

2. Experimental

2.1. Chemicals

Zinc(II) acetate ($ZnAc_2$, %), sodium sulfide ($Na_2S \times 9H_2O$, 99.99%), manganese(II) chloride ($MnCl_2 \times 4H_2O$, 99.99%), *L*-cysteine (Cys, > 97%), mercaptoacetic acid (> 99.0%, MAA), mercaptosuccinic acid (MSA, > 97%) and hydroxyl-terminated poly(amidoamine) dendrimer in methanol of third generation (PAMAM-$OH_{G=3}$) were purchased from Sigma-Aldrich Química S.A. (Spain). In all experiments deionized water was used.

2.2. Synthesis of ZnS:Mn coated with PAMAM-OH dendrimer

To obtain ZnS:Mn QDs, 2.5 mL of $ZnAc_2$ 0.1 M were mixed with 25 mL of Cys and MAA 0.02 M, used as ligand agent; and left stirred for 15 min, when were added 4 mL of $MnCl_2$ 0.01 M with continue stirring for 1 h. After this, previous addition of NaOH 1 M to adjust the pH at 11, was added 3.5 mL of Na_2S 0.1 M to be gently mixed. The crude reaction mixture was heated for 30 min at 90 °C and controlled by its fluorescence at 545 nm. After 48 h, the purification process was followed by the dialyzing of ZnS:Mn QDs for 6 h, precipitated with HCl 0.1 M, centrifuged, filtered and dissolved at pH 8.5, affording a fluorescent a colorless dissolution with at 595 nm.All experiments carried out were prepared with analytical grade reagents supplied from Sigma-Aldrich Química S.A. (Spain).

2.3. Characterization of ZnS:Mn coated with PAMAM-OH dendrimer

Fluorescence measurements were performed using a Jovin Yvon Fluoromax 4 TCSPC (Horiba), and measured between 400 and 700 nm using an integration time of 0.1 s and 5 nm slits for excitation and emission. Fluorescence lifetime analysis was done using an Edinburgh Instruments FLS920, equipped with a Xe lamp (450 W) as excitation source for steady state fluorescence measurements and monocromatics LEDs (PicoQuant PLS), controlled by a PDL 880-B system. Fluorescence decays were interpreted in terms of a multi-exponential: $I(t)=A+\Sigma B_i \exp^{-t/\tau i}$, where A and B_i are the pre-exponential factors and τ_i the decay times. Quantum yields (QY) of ZnS:Mn and ZnS:Mn@PAMAM-$OH_{G=3}$ were obtained using Rhodamine 6 G ($\Phi=0.93$ in methanol, $n=1.329$ and $\lambda_{ex}=535$ nm) as reference; ZnS:Mn and ZnS:Mn**@**PAMAM-$OH_{G=3}$ were dissolved in deionized water ($n=1.33$) and by 1, leads to obtain the QY of both nanoparticles (UV spectra is showed as Supporting Information Fig. SI1):

$$QY_{CDs} = QY_{st}\left[\frac{(dI/dA)_{CDs}}{(dI/dA)_{st}}\right]\left(\frac{n^2_{CDs}}{n^2_{st}}\right) \quad (1)$$

where *I* is the area under the fluorescence curves and A is the corresponding absorbance [32,33].

Transmission Electron Microscopy (TEM) and Energy Dispersive spectroscopy (EDAX) analysis were carried out with a Philips CM-200. X-ray photoelectron spectroscopic (XPS) studies were performed on a Physical Electronic PHI 5700 spectrometer using non-monochromatic MgK_α radiation (300 W, 15 kV, 1253.6 eV) for analyzing the core-level signals of the elements of interest with a hemispherical multichannel detector. The spectra of powdered samples were recorded with a constant pass energy value at 29.35 eV, using a 720 μm diameter circular analysis area. The X-ray photoelectron spectra obtained were analyzed using PHI ACESS ESCA-V6.0 F software and processed using Multipak 8.2B package. The binding energy values were referenced to adventitious carbon C 1 s signal (284.8 eV). Shirley-type background and Gauss-Lorentz curves were used to determine the binding energy. The size and zeta potential (ζ) of CDs were determined using a Zetasizer Nano ZS (Malvern Instruments, U.K.) equipped with a 4 mWHeNe laser operating at $\lambda=633$ nm. Size measurements were recorded with dynamic light scattering (DLS), at 25 °C in a polystyrene cell (ZEN0040) at a scattering angle of 173° and were average of three tests. The ζ measurements were also performed at 25 °C in polycarbonate folded capillary cells, incorporated with gold plated electrodes (DTS1061) and deionized H_2O was the dispersion medium. Both, size and ζ were automatically obtained by the software, using the Stokes-Einstein and the Henry equation, with the Smoluchowski approximation.

2.4. Fluorescence data analysis

For fluorescence data analysis of the different nanoparticles system which conform the ZnS:Mn coated by PAMAM-OH dendrimer, a series of emission spectra was collected, by excitation at different wavelengths, in the range 300–400 nm with 5 nm step. The emission spectra were measured in the range 400–670 nm, with 3 nm increment. In the analysis we used 4 matrices, corresponding to the pure ZnS, pure PAMAM-$OH_{G=3}$ dendrimer, ZnS:Mn and ZnS:Mn@PAMAM-$OH_{G=3}$. The artificial Raman bands were removed from the raw spectra by using the ale – UV–vis-IR Spectral Software 1.2, FluorTools, www.fluortools.com software. Each matrix was analyzed by using Multivariate Curve Resolution-Alternating Least Squares (MCR-ALS) method [34], which extracted the number of components, as well as their emission profiles. All analyses were performed using The Unscrambler software package (Camo ASA).

2.5. Atomic absorption spectroscopy

All the water samples were analyzed by AAS with a Cadmium (Cd) Lumina Hollow Cathode Lap. In 6 mL of water samples were acidified with 185 μL of 65% HNO_3 and the cadmium stock solutions were prepared by diluting different aliquots of a 1000 μg/mL cadmium standard stock solution. The measurements were done in a concentration range of 0.5–5 mg/L for the calibration curve with a linear regression of 0.9978.

2.6. Metal study

Previous the study of the enhancement effect of cadmium (Cd^{2+}), the metals As^{3+}, Ba^{2+}, Cd^{2+}, Co^{2+}, Cr^{3+}, Cu^{2+}, Fe^{3+}, Hg^{2+}, Mg^{2+}, Ni^{2+}, Pb^{2+}, Sb^{3+}, Tl^{+} and anions CN^-, CO_3^{2-}, SO_4^{2-} were studied by addition of 100 μL of the different metals stock solution (5×10^{-3} M) to 500 μL of ZnS:Mn@PAMAM-$OH_{G=3}$ to the desired concentrations levels in 1 mL of volume, filled up by H_2O. The solution mixture was then equilibrated at room temperature for 5 min before the spectral measurements at 448 and 595 nm. To check the selectivity of this sensor, the experiments were carried out with other metals ions including: Cu^{2+}, Fe^{3+}, Hg^{2+}, Pb^{2+}, Tl^{+} and Zn^{2+}, maintaining the same Cd^{2+} concentration (2.25×10^{-4} M) and ranging the metal ratio concentrations (1:1; 1:5; 5:1). The operation was exactly similar conditions that were used for the detection of Cd^{2+}; Data were obtained by the following

relationship (2):

$$Ratio = \frac{(I_{448}/I_{595})_{ZnS:Mn@PAMAM-OH:Cd-Metal}}{(I_{448}/I_{595})_{ZnS:Mn@PAMAM-OH:Cd}} \quad (2)$$

where ZnS:Mn**@**PAMAM-OH:Cd^{2+}-Metal is the ratio obtained when in dissolution are presented the proposed sensor with Cd^{2+} and the studied metal used as interference, and ZnS:Mn**@**PAMAM-OH:**Cd^{2+}** without metal assayed.

3. Discussion of the results

3.1. Synthesis and analysis of ZnS:Mn nanoparticles

Different parameters were studied to obtain the higher fluorescence intensity, the stabilizing agent, the pH and the concentration of the Mn^{2+} dopant. The planning experiments were drawn in the *Unscrambler* programme. The stabilizing agents studied were the Cys, MSA and MAA, all three had 0.02 M. The reactions were performed at different pH, at 7 and 11, and the concentration of Mn^{2+} was comprised between 0.179 and 0.833 mM, (Fig. SI2A) excited at 405 nm. Cys was selected at pH 11, the optimal value for ZnS nanoparticles. The heating time due to is well known factor to obtain larger size of nanoparticles was studied, and after the results obtained (Fig. SI2B) was observed that a time of 30 min was selected to obtain the best emission intensity. To obtain ZnS:Mn nanoparticles, a range of concentration for Mn^{2+} comprised between 0.179 and 0.833 mM was analyzed, being 0.179 mM the most intense signal under this proposal synthesis (Fig. SI2C).

After the dialyzing purification process, a red shift to 595 nm was observed in the emission spectra, excited at 345 nm (Fig. 1). For ZnS:Mn nanoparticles, two different emission bands are presented in the fluorescence spectra: the first emission band, at about 450 nm, also existed in the emission spectrum of the undoped ZnS nanocrystals. This emission band is due to the host ZnS but not from Mn^{2+} ions. Upon Mn^{2+} doping, a second characteristic emission band centered at around 595 nm is developed for the well-known $^4T_1 \rightarrow {}^6A_1$ d–d transition of Mn^{2+} ions on Zn^{2+} sites, where Mn^{2+} is tetrahedrally coordinated by S^{2-}. This can be explained as Mn^{2+} incorporated into the ZnS lattice led to the Mn^{2+} based orange emission while ZnS with surface bound Mn^{2+} yielded the ultraviolet emission. Thus, it could be concluded that the Mn^{2+} ions in our samples were incorporated into the host ZnS nanocrystals [35,36].

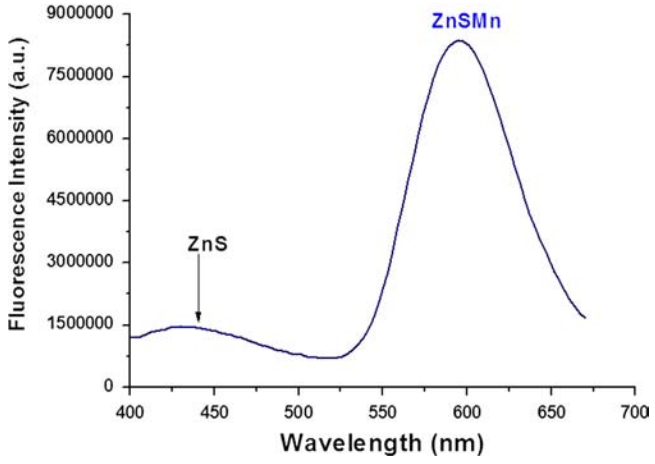

Fig. 1. Fluorescence spectra of dialyzed ZnS:Mn^{2+} with [Mn^{2+}]=0.179 M at pH 11 and coated with Cys (0.02 M) after 30 min of heat. Excitation at 345 nm.

3.2. Characterization of ZnS:Mn nanoparticles

The size and morphology of ZnS:Mn nanoparticles were characterized by TEM (Fig. 2), where nearly monodispersed cores were obtained with an average diameter of 4 nm and revealed packs of parallel willing with a high regular disposition, inset in Fig. 2 is showed the inter-planar distance 0.30 nm which agreed well with obtained previously [37]. The average hydrodynamic size was 17.33 ± 4.97 nm from DLS data (Fig. SI3), thus suggesting that the nanoparticles dispersed well in water. The hydrodynamic diameters were larger than those of the cores due to the solvation layer around the QDs in aqueous solution. Later analysis was obtained the size from DLS data for ZnS:Mn@PAMAM-$OH_{G=3}$, which provided a value of 19.50 ± 4.24 nm. The nanoparticles were subjected to EDAX analysis (Fig. SI4) which shows the general composition of ZnSMn studied, thus clearly shows the presence of Mn^{2+} (0.62%), Zn (19.04%) and S (80.34%), supporting that Mn^{2+} ion was incorporated by substitution into the ZnS host lattice and confirmed by XPS analysis. The negative ζ of ZnS:Mn nanoparticles (-19.90 ± 0.50 mV) is due to the presence of deprotonated cysteine groups on the nanoparticles surface (pK_a(α–NH_3^+)=10.78 and pK_a (–CH_2-SH)=8.33, consistent with the pH of the synthesis procedure. The ATR spectra analysis showed (Fig. SI5) three main broad bands which are assigned at 1629 cm^{-1} (–COO^-), the band with a shoulder comprised between 3000–3500 cm^{-1} (–OH and N–H) and the weak broad band at 2130 cm^{-1} is assigned at the stretching band of the S-H, which is indication of the low vibration of the covalent bond formed with the ZnS QDs. In the same figure, the spectra of the coated nanoparticles with PAMAM-$OH_{G=3}$ are overlapped, where the only difference is the presence of two bands at 2365 and 2344 cm^{-1}.

3.3. XPS analysis

The XPS study of the ZnS:Mn nanoparticles stabilized with cysteine gives relevant information concerning the surface of the nanoparticles. The C 1*s* core level spectrum (Fig. SI6A) can be decomposed into three contributions at 284.8 eV (75%), 286.1 eV (15%) and 288.1 eV (10%). This spectrum is more or less similar to that of L-cysteine reported in the literature [38] were three contributions at 285.2, 286.7 and 288.5 eV was reported. The first contribution at low binding energy (284.8 eV) is assigned, in addition of adventitious carbon, to C-S- groups. The second at 286.1 eV is mainly due to C-NH_2 and present an area slightly higher than that of the third contribution at 288.1 eV due to the carboxylate group. The S 2*p* core level spectrum (Fig. SI6B) shows a single peak with the doublet S $2p_{3/2}$ and S $2p_{1/2}$ at 161.1 and 162.3 eV, respectively. This signal is assigned to sulfur as thiolated [38], and free thiol groups were not observed in the S 2*p* core level spectrum (signal at about 164 eV). The N 1*s* spectrum (not shown here) shows a maximum at about 400.0 eV and is assigned, as expected, to the amino group of cysteine. The Zn $2p_{3/2}$ core level spectrum shows a single symmetric maximum centered at 1021.2 eV (Fig. SI6C). This peak is not very informative concerning the chemical state of Zn, for this reason the $ZnL_3M_{4,5}M_{4,5}$ Auger spectrum was also registered (Fig. SI6D). In this way is possible to calculate the modified Auger parameter (α') according 3. This Auger signal is sensitive to the chemical state of zinc, and two contribution were observed at 260.9 eV (26%) and 263.7 eV (74%).

$$\alpha' = 1253.6 + KE(ZnLMM) - KE\left(Zn\ 2p_{3/2}\right) \quad (3)$$

where KE(ZnLMM) is the kinetic energy of the Auger electron of ZnLMM and KE(Zn $2p_{3/2}$) the kinetic energy of the photoelectron Zn $2p_{3/2}$, and 1253.6 eV is the energy of the excitation source.

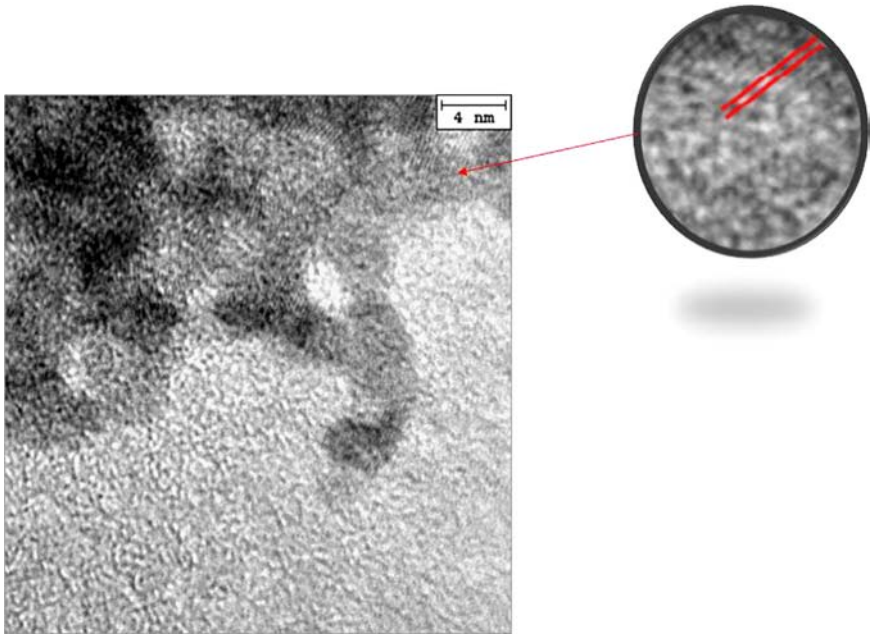

Fig. 2. TEM image of ZnS:Mn 4 nm of average diameter (Inset a magnification of the inter-planar distance of 0.30 nm).

The calculated α' values were 2013.9 and 2011.1 eV, respectively. And using the correspondent Wagner's diagram [39], the presence of a core of ZnS ($\alpha'=2011.2$ eV) in the nanoparticles with Zn bonded to surface cysteine through the thiol group ($\alpha'=2013.9$ eV) is suggested. The Mn 2*p* signal (not shown) is very weak, showing a photoemission Mn $2p_{3/2}$ at 640.3 eV. This value is similar to that reported at 640.4 eV for MnS [39] C: 46.42%, O: 16.31%, N: 3.60, S: 18.15%, Cl 1.49%, Mn: 0.13% and Zn 13.90%. This composition also indicates that part of sulfur is forming part of the metallic sulfide and the excess corresponds to the thiolated groups. The coexistence of metallic Zn and ZnO was confirmed, although it was not possible to distinguish between the single metallic Zn^0 and the alloyed Zn^0.

3.4. Functionalization with PAMAM-$OH_{G=3}$

Two families and generations of dendrimers, PAMAM with hydroxyl terminal groups (PAMAM-$OH_{G=2,\ 3,\ 5}$) and thiol-terminated DAB dendrimers ($DAS_{G=2-5}$) have been assayed, to analyze the influence of the addition to ZnS nanoparticles (Fig. SI7). As observed, all dendrimers conferred a protective environment to ZnS nanoparticles, as observed in the fluorescence intensity, which is most increased in the presence of PAMAM-$OH_{G=2,3}$. It was observed that the hydroxyl dendrimer derivates (PAMAM-$OH_{G=3,5}$) showed fluorescence emission by theirselves, explained by their synthesis procedure (Fig. SI8) [40], being selected PAMAM-$OH_{G=3}$ which showed for a hand a higher fluorescence intensity (Fig. SI9) and low influence on the emission band at 595 nm when added at different concentration to ZnS:Mn nanoparticles (Fig. 3).

The conjugation of PAMAM-$OH_{G=3}$ with ZnS:Mn is not a typically fluorescence resonance energy transfer (FRET) because both raw and coupled bands remained practically immutable, as proof the quantum yield (Φ) for ZnS:Mn and ZnS:Mn@PAMAM-$OH_{G=3}$ are 0.1470 and 0.1509, respectively, in methanol solution. The fluorescence mechanism could not be supported by the donor-acceptor excitons transfer because PAMAM-$OH_{G=3}$ itself presents fluorescence at 448 nm and the doped QD at 595 nm, when the dendrimer is added to the doped QD, the zinc can form stable complexes with dendrimer trough its interior amino groups rather

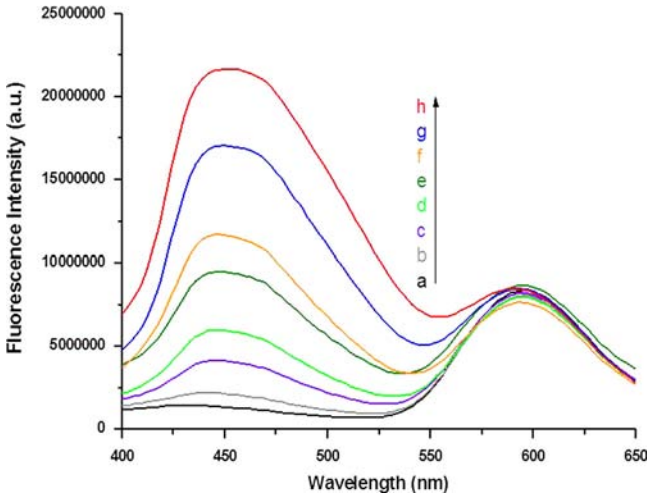

Fig. 3. Influence of the concentration of PAMAM-$OH_{G=3}$ on the fluorescence intensity of ZnS:Mn^{2+}: (a) 0 M; (b) 4.07×10^{-8} M; (c) 2.04×10^{-7} M; (d) 4.07×10^{-7} M; (e) 8.14×10^{-7} M; (f) 1.22×10^{-6} M; (g) 2.44×10^{-6} M and (h) 4.07×10^{-6} M. Excitation at 345 nm.

than exterior hydroxyl groups [41]. Probably, due to the binding nature between PAMAM-$OH_{G=3}$ and ZnS:Mn, the chemical relation which they have is mainly about donor-acceptor electrons and at quantum level a reduced donor-acceptor excitons effect, maintaining the fluorescent signals of raw and coupled bands almost equal. The effect of ionic strength on fluorescence was analyzed, by using increasing concentration of NaCl (between 0 and 2 M), showing a decreasing about 57% in the intensity when NaCl concentration does increase, even though at small concentration, indicating the moderate tolerance of ZnS:Mn@PAMAM-$OH_{G=3}$ (Fig. SI10).

The effect of pH (4-11) on the fluorescence intensity was studied, and was compared with ZnS:Mn, showing the similar behavior. With increasing the pH from 6.04 to 6.90 a drastic decreasing of the intensity (60%) is observed, for ZnSMn, but when is analyzed ZnS:Mn@PAMAM-$OH_{G=3}$, this drastic decrease was observed at 8.72 (Fig. SI11). Similar behavior at different values is

found when coated by the dendrimer but, the decrease occurs at slightly high pH, explained that dendrimer coating process protect from the environment.

3.5. Component analysis of ZnS:Mn@PAMAM-OH$_{G=3}$ by MCR-ALS

The results of MCR-ALS analysis of the emission profiles for pure ZnS, pure PAMAM-OH$_{G=3}$ dendrimer, ZnS:Mn and ZnS:Mn@PAMAM-OH$_{G=3}$ are included in Fig. 4. The emission spectrum of ZnS contains four components with the maxima at 439, 493, 535 and 595 nm. After complexation with Mn^{2+}, the first three components of ZnS disappear due to the formation of a new compound, and the new components are formed at 472, 556, 589 and 643 nm. The fourth ZnS component stays unchanged. The PAMAM-OH spectrum contains two contributions at 454 and 465 nm. In the spectrum of ZnS:Mn@PAMAM-OH$_{G=3}$ five components can be observed. The one PAMAM-OH component, at 454 nm, stays unchanged, while its second component is blue shifted for 20 nm, at position 445 nm. The other three components, at 556, 589 and 643 nm come from ZnSMn and are unchanged in the complex with PAMAM-OH. This shows that PAMAM-OH does not change structure of ZnSMn, and change of the one PAMAM-OH component is due to binding to ZnSMn. This is evidence that the formed complex is stable.

3.6. Fluorescence enhancement with Cd^{2+} ions. Ratiometric sensor of Cd^{2+}

Previous the study of the enhancement effect of cadmium (Cd^{2+}), a screening of metals were performed, to analyse the response of the proposed ZnS:Mn@PAMAM-OH$_{G=3}$, used as metal sensor. When no metal ion was added to the solution, the emission profile could be summarized at 448 and 592 nm, being this band where the most interesting results are obtained when added the metals to the solution (Fig. 5).

The effect found are the enhancement due to Tl^{+} (20.2) and Cd^{2+} (32.1), being this metal which offered a significant enhancement of the signal at 595 nm (2 folds), when compared with the others metals added in separated experiments. No significance changes in the intensity was found when added As^{3+} (4.9), Ba^{2+} (1.4), CN^{-} (1.6), CO_3^{2-} (2.8), Mg^{2+} (1.2) and SO_4^{2-} (1.0), moderated for Co^{2+} (11.1), Cr^{3+} (8.6), Ni^{2+} (11.8) and Sb^{3+} (6.2). Metal ions such as Cu^{2+} (18.3), Fe^{3+} (56.9), Hg^{2+} (69.7) and Pb^{2+} (73.1) could cause a larger quenching effect (the values presented in parenthesis represents the mean variation of fluorescence intensity, in percentage, (Fig. 6). Due to the enhancement on the fluorescence intensity effect found and the concern of the Cd^{2+} in the environment was considered the most interesting metal ion to be studied. In Section 2.5 the relationship to obtain the data obtained is detailed.

The concentration effect of Cd^{2+} was studied in the range comprised between 5×10^{-5} and 2.5×10^{-3} M (Fig. SI12A). Under the optimum conditions, the change in the fluorescence intensity at 595 had a prominent linear relationship ($r > 0.999$) with the concentration of Cd^{2+} over the range 1.225×10^{-5}–6.75×10^{-4} M. The inset in Fig. SI12A indicates the correlation of the intensity ratios of emission at 448 nm to 595 nm (I_{448}/I_{595}). When was observed the effect in the two bands studied, is possible to justify that the functionalization of ZnSMn by PAMAM-OH$_{G=3}$ dendrimer is a good approach, (Fig. SI12B and C), where are represented the influence on the fluorescence intensity of ZnS:Mn@PAMAM-OH$_{G=3}$ at different Cd^{2+} concentrations, observed at 595 nm (Fig. SI12B) when compared with raw ZnSMn nanoparticles, and 450 nm (Fig. SI12C) respectively when is compared with raw PAMAM-OH$_{G=3}$, which demonstrated the effective functionalization of ZnSMn and its potential use as ratiometric sensor of Cd^{2+}, always the presence of the dendrimer in the system improve the analytical signal. In both cases, the fluorescence intensity of ZnS:Mn**@**PAMAM-OH$_{G=3}$ increased at 448 nm and 595 nm comparing with raw PAMAM-OH$_{G=3}$ and raw ZnS:Mn bands. At 448 nm, the fluorescence intensity of ZnS:Mn@PAMAM-OH$_{G=3}$ is higher than raw PAMAM-OH$_{G=3}$, even at low concentrations of Cd^{2+}. At 595 nm, the fluorescence intensity of ZnS:Mn@PAMAM-OH$_{G=3}$ is higher than doped QDs from 110 μM of Cd^{2+}, giving the same fluorescent response below. This probably demonstrates the preferential binding of Cd^{2+} for the thiol group of Cys rather than amino groups of PAMAM-OH$_{G=3}$ dendrimer. When the Cd^{2+} ions complexed with thiol groups, the signal of ZnS:Mn and PAMAM-OH$_{G=3}$ is enhanced due to a charge transfer between a Cd^{2+}@ZnS:Mn and the ZnS:Mn@PAMAM-OH$_{G=3}$, until a point where the thiol groups are fully complexed and the remaining Cd^{2+} starts to complex with amino groups of the dendrimer, quenching the signal of PAMAM- OH$_{G=3}$ and saturating the signal of ZnS:Mn. The proposed sensor was optimized to obtain the best sensitivity. The limit of detection (LOD) and quantification (LOQ=3 × LOD) were 24.334 and 81.114 μM, respectively, with an accuracy as relative standard deviation (RSD, n= 10)=4.07%, as analytical Figures of merit.

Previously to this work, our group did a similar study involving nanocomposites of QDs and dendrimers for the detection of Cd^{2+} ions by using CdSe QDs functionalized with thiolated DAB dendrimer of generation 5. The same fluorescent response behavior of enhancement was obtained and the S-DAB-G5-CdSe sensor emitted a single band at 535 mm (λ_{ex}=408 nm) and a LOD of 10.08 μM [26]. Another analytical example for the detection of Cd^{2+} involved the use of MPA-capped CdTe QDs and the sensing was obtained by enhancing the fluorescent signal with free Cd^{2+} ions at 615 nm (λ_{ex}=350 nm), the LOD founded was 0.5 μM [42]. Beside of the ZnS:Mn@PAMAM-OH$_{G=3}$ sensor has a superior LOD than the S-DAB-G5-CdSe nanocomposites and the MPA-capped CdTe QDs, the proposed sensor for Cd^{2+} detection has a huge advantage of being free of cadmium, avoiding the toxicological problems associated to the cadmium-based QDs (Table 1).

3.7. Tolerance to interferences metal ions

To assess the possibility of analytical application of the present nanosensor, the effects of different concentration ratios of several cations, that may be presented in real samples, on the fluorescence intensity of ZnS:Mn@PAMAM-OH$_{G=3}$ with Cd^{2+} (2.25×10^{-7} M), was studied – Cu^{2+}, Fe^{3+}, Hg^{2+}, Pb^{2+}, Tl^{+} and Zn^{2+}. The fluorescence intensities of ZnS:Mn@PAMAM-OH$_{G=3}$, at different concentration ratios versus M^{n+}, (5:1; 1:1 and 1:5) were measured in separate sets of experiments and summarized in Table 2. Where ZnS:Mn@PAMAM-OH:**Cd**is the ratio obtained when in dissolution are presented the proposed sensor with Cd^{2+} and the studied metal used as interference, and ZnS:Mn@PAMAM-OH:**Cd^{2+}** without metal assayed. In all the cases analyzed, it was found a quenching effect on the signal of ZnS:Mn@PAMAM-OH:**Cd^{2+}**, obtaining a moderate behavior. The most pronounced effect was for Pb^{2+} with a signal decreased over 50–70%.

Fig. SI13A and B shows the results of MCR-ALS analysis of the emission profiles for ZnS:Mn@PAMAM-OH$_{G=3}$ complex in presence of Cd^{2+} ions. The emission spectrum contains three components. The components at 454 and 589 nm have the same position as in the complex in absence of Cd. The components at 454, 556 and 643 nm of the complex disappeared in the presence of Cd, while a new component appeared at 583 nm (Figs. 4 and SI13). This indicates that Cd induced certain structural changes of the complex. A conformation change may be proposed, having in mind a branched structure of the complex due to the PAMAM-OH dendrimer.

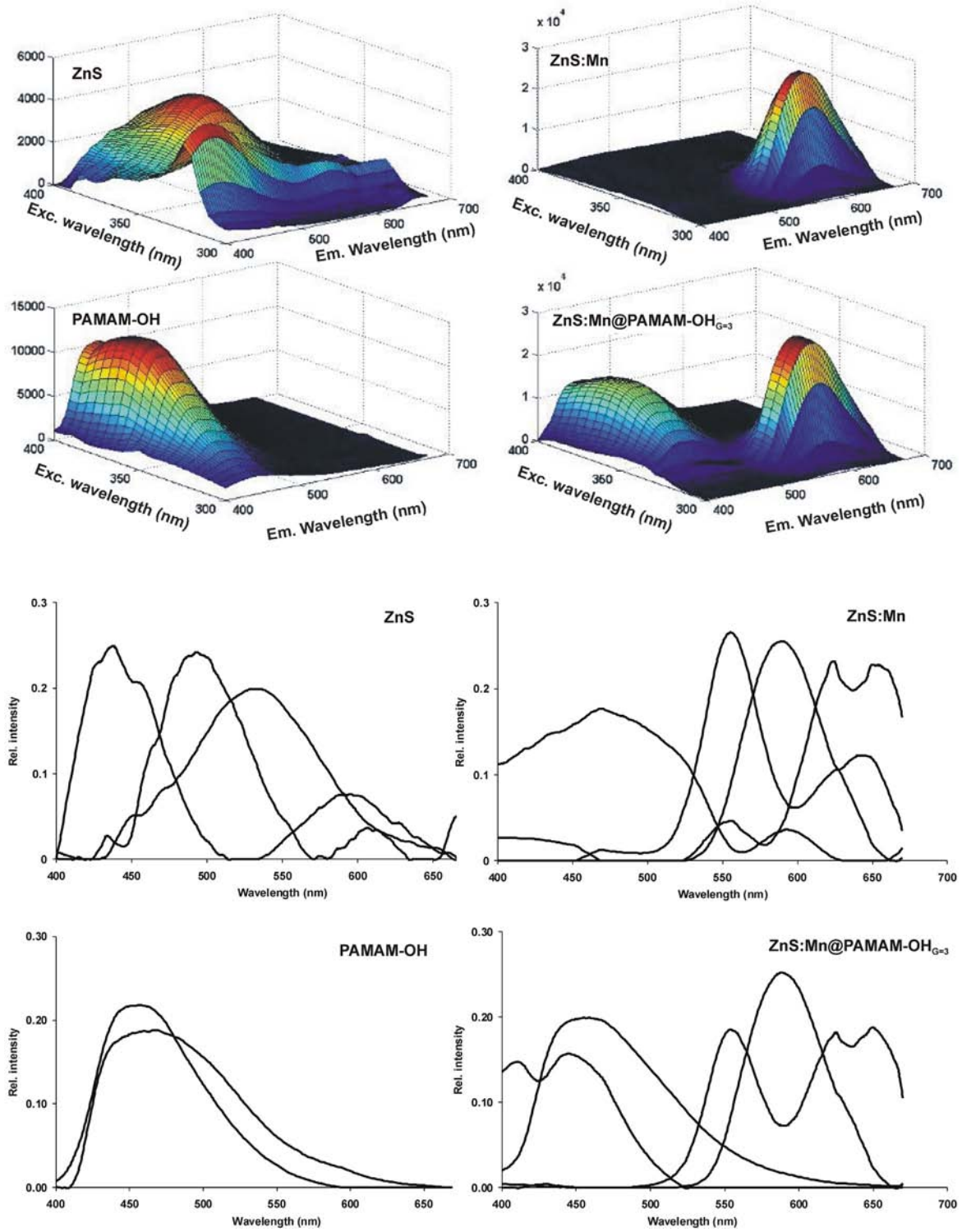

Fig. 4. Upper panel: Excitation-emission matrix for the raw spectra of ZnS, ZnS:Mn, PAMAM-OH and ZnS:Mn@PAMAM-OH$_{G=3}$; Lower panel: Estimated emission profiles for ZnS, ZnS:Mn, PAMAM-OH and ZnS:Mn@PAMAM-OH$_{G=3}$.

3.8. Application to drinking water

Due to the possibility of contamination in drinking water by Cd^{2+}, as result of an impurity from the Zn^{2+} or the galvanized pipes or Cd^{2+} containing solders in fittings, water heaters, water coolers and taps. Therefore, as application, were spiked different concentrations of Cd^{2+} in tap water, bottled water, river water and sewage. The results were compared with Cd^{2+} concentrations measured by Atomic Absorption Spectroscopy (AAS) and are presented in Table 3. In average, the results obtained by the proposed ratiometric sensor have a slight deviation (less than 10%) concerning to the Cd^{2+} concentrations measured by AAS, for the same samples. Comparing the precision of the two analytical methods, the ZnS:Mn@PAMAM-OH$_{G=3}$ sensor showed a mean precision of 5.88% ± 2.45% instead of the 1.41% ± 0.76% for the AAS, this probably occurs because of the huge active sites of dendrimer

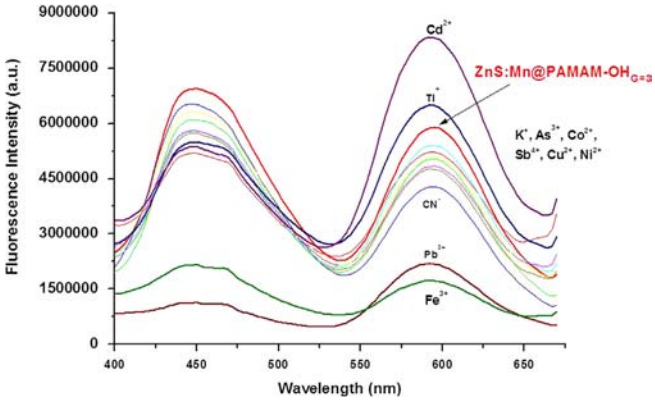

Fig. 5. Fluorescence spectra of ZnS:Mn@PAMAM-OH$_{G=3}$ upon addition of metal ions (7.5×10^{-7} M). excited at 405 nm.

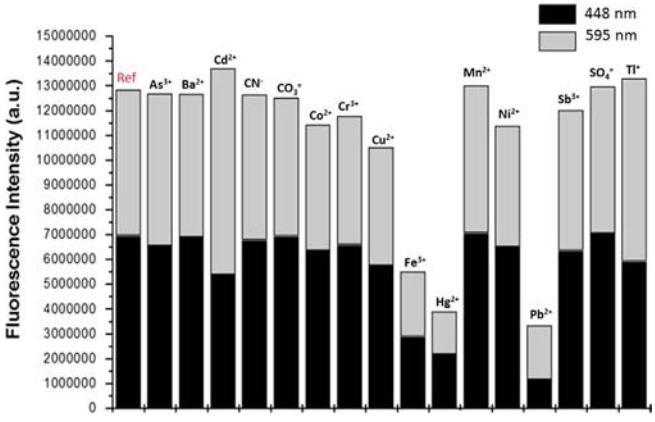

Fig. 6. Ratio of tolerance of the interferences species on the fluorescence spectra at 488 and 595 nm of ZnS:Mn@PAMAM-OH$_{G=3}$ excited at 405 nm.

Table 1
Analytical parameters for Cd^{2+} determination.

LOD (μM)	LOQ (μM)	RSD (%)	Sensitivity
23.44 ± 0.69	78.11 ± 2.26	5.78 ± 2.42	0.034 ± 0.001
Dynamic range: 2.34×10^{-5}–1.10×10^{-3} M			

Table 2
Tolerance ratio of ZnS:Mn@PAMAM-OH$_{G=3}$ when is dissolved Cd^{2+} (2.25×10^{-7} M) versus other metals as interference at different ratios.

	5:1	1:1	1:5
Cu^{2+}	0.65 ± 0.12	0.73 ± 0.09	0.81 ± 0.07
Fe^{3+}	0.84 ± 0.05	0.98 ± 0.02	0.85 ± 0.05
Hg^{2+}	0.61 ± 0.11	0.64 ± 0.12	0.83 ± 0.05
Pb^{2+}	0.53 ± 0.18	0.37 ± 0.32	0.43 ± 0.20
Tl^{+}	0.62 ± 0.10	0.59 ± 0.20	0.56 ± 0.15
Zn^{2+}	0.61 ± 0.12	0.59 ± 0.14	0.53 ± 0.12

were the Cd^{2+} can be complexed, generating signals with light deviations.

4. Conclusions

Summarizing, we have explored the ratiometric behavior of ZnS:Mn^{2+} fluorescent nanoparticles when they are synthesized by a novel method and the further functionalization with hydroxyl terminated PAMAM dendrimer, and used as sensor probe for Cd^{2+}. Two emission bands at 448 and 595 nm were used to obtain the ratiometric ratio (I_{448}/I_{595}). By a wide of analytical techniques was characterized which concluded the presence of Mn^{2+} in the ZnS lattice which produces the orange emission under UV light. The presence of dendrimer in the surface of ZnS:Mn^{2+} increase the QY and the stability when was studied the pH dependence. The main conclusion after fluorescent component analysis was that no influence in the ZnS:Mn structure after coating with dendrimer. When used as sensor probe for Cd^{2+}, an enhancement of the band at 595 nm obtaining prominent linear relationship which was used for metal analysis in water.

An available alternative to fluorescent sensors based on cadmium-made QDs in the detection of free Cd^{2+} ions in real water samples.

Table 3
Comparation of Cd^{2+} measurements in different real water samples by AAS and ZnS:Mn@PAMAM-OH$_{G=3}$ sensor.

Water samples	$[Cd]_{AAS}$ (ppm)	$[Cd]_{Ir}$ (ppm)	Accuracy (%)
Tap	18.48 (0.25)**	16.89 (1.40)	8.59
	27.86 (0.27)	25.26 (1.72)	9.34
	36.49 (0.74)	36.65 (1.50)	0.44
	46.56 (0.19)	46.02 (1.89)	1.15
Bottled	15.07 (0.20)	15.15 (1.35)	0.50
	27.03 (0.57)	25.16 (1.41)	6.93
	37.72 (0.54)	34.33 (1.10)	8.99
	46.88 (0.14)	44.19 (1.28)	5.73
River	14.97 (0.18)	14.30 (1.36)	4.51
	28.12 (0.38)	30.30 (1.79)	7.74
	33.94 (0.20)	31.98 (1.31)	5.80
	45.08 (0.89)	43.57 (1.52)	3.36
Sewage	15.47 (0.49)	17.09 (1.83)	10.50
	27.24 (0.56)	27.77 (2.05)	1.96
	37.45 (0.22)	38.16 (1.91)	1.89
	46.03 (0.81)	42.93 (1.76)	6.72

*Means of three different determinations.
** Standard deviation in parenthesis.

Acknowledgments

Authors are gratefully to Grant SFRH/BD/84318/2012 to FCT (Lisbon, Portugal) and Grant 173017 from the Ministry of Education, Science and Technological development of the Republic of Serbia.

Appendix A. Supporting information

Supplementary data associated with this article can be found in the online version at http://dx.doi.org/10.1016/j.talanta.2014.10.010.

References

[1] D. Mocatta, G. Cohen, J. Schattner, O. Millo, E. Rabani, U. Banin, Science 332 (2011) 77.
[2] R. Zhang, W. Chen, Biosens. Bioelectron. 55 (2014) 83.
[3] J. Ju, W. Chen, Biosens. Bioelectron. 58 (2014) 219.
[4] P. Wu, X.P. Yan, Chem. Soc. Rev. 42 (2013) 5489.
[5] J. Planelles-Aragó, B. Julián-López, E. Cordoncillo, P. Escribano, F. Pellé, B. Viana, C. Sanchez, J. Mater. Chem 18 (2008) 5193.
[6] S. Sarkar, A.R. Maity, N.S. Karan, N. Pradhan, J. Phys. Chem. C 117 (2013) 21988.
[7] D.J. Norris, N. Yao, F.T. Charnock, T.A. Kennedy, Nano Lett. 1 (2001) 3.
[8] M. Behboudnia, P. Sen, Phys. Rev. B 63 (2001) 035316.
[9] A.A. Bol, A. Meijerink, J. Lumin. 87–89 (2000) 315.
[10] A.A. Bol, A. Meijerink, J. Phys. Chem. B 105 (2001) 10197.

[11] C. Jin, J. Yu, L. Sun, K. Dou, S. Hou, J. Zhao, Y. Chen, S. Huang, J. Lumin. 66–67 (1995) 315.
[12] N. Karar, F. Singh, B.R. Mehta, J. Appl. Phys. 95 (2004) 656.
[13] S. Sapra, A. Prakash, A. Ghangrekar, N. Periasamy, D.D. Sarma, J. Phys. Chem. B 109 (2005) 1663.
[14] H. Mattousi, J.M. Mauro, E.R. Goldman, G.P. Anderson, V.C. Sundar, F.V. Mikulec, M.G. Bawendi, J. Am. Chem. Soc. 122 (2000) 12142.
[15] M. Gaceur, M. Giraud, M. Hemadi, S. Nowak, N. Menguy, J.P. Quisefit, K. David, T. Jahanbin, S. Benderbous, M. Boissière, S. Ammar, J. Nanopart. Res. 14 (2012) 932.
[16] Y. Shang, L. Qi, F.Y. Wu, Microchim. Acta 177 (2012) 333.
[17] L. Zhu, S. Ang, W.T. Liu, Appl. Environ. Microbiol. 70 (2004) 597.
[18] W.Y. Xie, W.T. Huang, H.Q. Luo, N.B. Li, Analyst 137 (2012) 4651.
[19] T. Zhao, X. Hou, Y.N. Xie, L. Wu, P. Wu, Analyst 138 (2013) 6589.
[20] B.H. Zhang, L. Qi, F.Y. Wu, Microchim. Acta 170 (2010) 147.
[21] P. Wu, Y. He, H.F. Wang, X.P. Yan, Anal. Chem. 82 (2010) 1427.
[22] H. Yan, H.F. Wang, Anal. Chem. 83 (2011) 8589.
[23] M. Geszke-Moritz, H. Piotrowska, M. Murias, L. Balan, M. Moritz, J. Lulek, R. Schneider, J. Mater. Chem. B 1 (2013) 698.
[24] S. Baruah, G. Tumcharern, J. Dutta, Adv. Mat Res. 55–57 (2008) 589.
[25] H.Y. Kong, B.K. Song, J. Byun, C.S. Hwang, Bull. Kor. Chem. Soc. 34 (2013) 1181.
[26] M. Algarra, B.B. Campos, D. Gomes, B. Alonso, C.M. Casado, M.M. Arrebola, M.J. Diez de los Rios, M.E. Herrera-Gutiérrez, G. Seller-Pérez, J.C.G. Esteves da Silva, Talanta 99 (2012) 574.
[27] M. Algarra, B. Campos, B. Alonso, M.S. Miranda, A.M. Martínez, C.M. Casado, J.C.G. Esteves da Silva, Talanta 88 (2012) 403.
[28] D Yamamoto, T. Koshiyama, S. Watanabe, M.T. Miyahara, Coll. Sur. A: Phsicochem. Eng. Aspects 411 (2012) 12.
[29] N. Chen, Y. He, Y. Su, X. Li, Q. Huang, H. Wang, X. Zhang, R. Tai, C. Fan, Biomaterials 33 (2012) 1238.
[30] Y. Wei, H. Hao, J. Zhang, X. Hao, C. Dong, Anal. Methods 6 (2014) 3227.
[31] Y. Park, C. Koo, H.Y. Chen, A. Han, D.H. Son, Nanoscale 5 (2013) 4944.
[32] A.M. Brouwer, Pure Appl. Chem. 83 (2011) 2228.
[33] G. Weber, F.W.J. Teale, Trans. Faraday Soc. 53 (1957) 646.
[34] M. Algarra, K. Radotić, A. Kalauzi, B. Alonso, C.M. Casado, J.C.G. Esteves da Silva, Talanta 105 (2013) 267.
[35] R. Beaulac, P.I. Archer, D.R. Gamelin, J. Solid State Chem. 181 (2008) 1582.
[36] K. Sooklal, B.S. Cullum, S.M. Angel, C.J. Murphy, J. Phys. Chem. 100 (1996) 4551.
[37] R. Ban, J. Li, J. Cao, P. Zhang, J. Zhang, J.J. Zhu, Anal. Methods 5 (2013) 5929.
[38] O. Cavalleri, L. Oliveri, A. Dacca, R. Paroli, R. Polandi, Appl. Surf. Sci. 175–176 (2001) 357.
[39] J.F. Moulder, W.F. Stickle, P.E. Sobol, K.D. Bomben, J. Chastain (Eds.), Handbook of X-ray Photoelectron Spectroscopy, Perkin-Elmer Corporation Eden Prairie, 1992, p. 204.
[40] D. Wang, T. Imae, J. Am. Chem Soc. 126 (2004) 13204.
[41] A.B. Nepomnyashchii, M.A. Alpuche-Aviles, S. Pan, D. Zhan, F.R.F. Fan, A.J. Bard, J. Electroanal. Chem. 621 (2008) 286.
[42] H. Xu, R. Miao, Z. Fang, X. Zhong, Anal. Chim. Acta 687 (2011) 82.